Hindawi Publishing Corporation
International Journal of Photoenergy
Volume 2010, Article ID 389182, 7 pages
doi:10.1155/2010/389182

Research Article

Pt/Mesoporous Carbon Counter Electrode with a Low Pt Loading for High-Efficient Dye-Sensitized Solar Cells

Guiqiang Wang, Junfeng Gu, and Shuping Zhuo

School of Chemical Engineering, Shandong University of Technology, Zibo 255049, China

Correspondence should be addressed to Guiqiang Wang, wgqiang123@163.com

Received 29 March 2010; Revised 27 May 2010; Accepted 19 June 2010

Academic Editor: Nicolas Alonso-Vante

Pt/Mesoporous carbon counter electrodes with a low Pt loading for dye-sensitized solar cells were fabricated by coating Pt/mesoporous carbon on fluorine-doped tin oxide glass. Pt/mesoporous carbon samples were prepared by reducing H_2PtCl_6 with $NaBH_4$ in mesoporous carbon and characterized by N_2 adsorption analysis, X-ray diffraction, X-ray photoelectron spectroscopy, and transmission electron microscopy. The Pt particles deposited on mesoporous carbon support were found to be in uniform shape and narrow range of particle size. Low-Pt-loading Pt/mesoporous carbon counter electrode showed a high electrocatalytic activity for triiodide reduction. Electrochemical impedance spectroscopy measurement displayed a low charge-transfer resistance of 1.2 Ωcm^2 for 1-Pt/mesoporous carbon counter electrode. Dye-sensitized solar cells based on the 1-Pt/mesoporous carbon counter electrode achieved an overall conversion efficiency of 6.62% under one sun illumination, which is higher than that of the cell with the conventional Pt counter electrode.

1. Introduction

Dye-sensitized solar cells (DSCs) composed of a dye-sensitized nanocrystalline TiO_2 photoanode, an electrolyte containing a redox couple of I^-/I_3^- and a counter electrode, have aroused intensive interest in transferring solar energy to electricity due to their low cost, simple preparation procedure, and relatively high efficiency [1–3]. In such cell, the redox reactions occur on the interface of electrolyte/counter electrode and electrolyte/dye molecule. The reaction on the surface of counter electrode is the reduction of triiodide such as $I_3^- + 2e \rightarrow 3I^-$, while the oxidation of iodide occurs on the dye molecule [4, 5]. Therefore, the counter electrode must be well conducting and exhibit a high electrocatalytic activity for the reduction of triiodide.

Up to now, Pt has been the preferred material for counter electrode due to its excellent catalytic activity for reduction of triiodide, high conductivity and high thermal and chemical stability [6–8]. However, Pt is one of the expensive component materials in DSCs. In order to reduce the production cost of DSCs, several varieties of carbonaceous materials such as carbon nanotubes [9–13], activated carbon [14], carbon black [15], and hard carbon spherule [16] have been used as the attractive low-cost substitute for Pt. In recent years, conducting polymers have also been employed as catalyst on fluorine-doped tin oxide (FTO) glass for counter electrode of DSCs [17, 18]. While the cost of conducting polymers is lower than that of Pt, lack of adhesion to the transparent conducting substrate poses a long-term stability risk.

Recently, some researches are focused on reducing the Pt loading on counter electrode by increasing the Pt utilization without sacrificing the performance [19, 20]. The increase of Pt utilization can be achieved through using Pt nanoparticles which can increase the surface-to-mass ratio and adopting the conducting support with high specific surface area [21, 22]. Since carbon supports have advantages of high conductivity, high specific surface area, and high stability, carbons with nanostructure have been paid attention as catalyst supports [23]. Among a variety of nanostructured carbons, mesoporous carbon (MC) is highly intriguing because of their accessible porosity and large pore volumes [24, 25]. In our previous study, it was found that the pure MC was suitable as the counter electrode of DSCs [26]. However, the MC counter electrode usually requires a thick

carbon film to obtain an acceptable catalytic activity. In this paper, Pt nanoparticles supported on MC were prepared and employed to fabricate Pt/MC counter electrode with a low Pt loading. An overall conversion efficiency of 6.62% was obtained for the DSCs with Pt/MC counter electrode, indicating the great promise in DSCs.

2. Experimental

MC materials were prepared by the self-organization of surfactant and carbon precursors, followed by carbonization. Briefly, triblock copolymer Pluronic F127 (9 g) was dissolved in the mixture of water (43 g) and ethanol (57 g), and then phloroglucinol (16 g) was added. After complete dissolution of phloroglucinol, formaldehyde (16 g, 37 wt%) was added to the above solution. Finally, HCl (0.3 mL, 0.5 N) was added as a catalyst. This mixture was stirred at 30°C for 30 minutes, and then heated at 100°C for 8 hours in order to promote the polymerization between phloroglucinol and formaldehyde. The resulted samples were heated at 400°C for 3 hours and further 800°C for 6 hours under a nitrogen atmosphere. Finally, MC materials were obtained.

Pt was loaded on MC by aqueous impregnation using $NaBH_4$ as the reducing agent. MC materials were first grounded using planetary ball mill. Then, 300 mg of MC powder and 5 mL of isopropanol were added to 150 mL of twice distilled water and ultrasonicated for 20 minutes. The H_2PtCl_6 solution with predetermined Pt/MC ratio (0.5, 1, and 2 wt%) was added into MC suspension and ultrasonically stirred for 30 minutes, followed by adding 0.5 M of $NaBH_4$ solution ($NaBH_4$ were excess to reduce H_2PtCl_6 fully) and the ultrasonically stirring for 2 hours. The resulted slurry was filtered, washed several times, and then dried at 70°C in a vacuum oven. Finally, the catalyst samples were calcined at 350°C for 30 minutes. The Pt/MC samples with Pt/MC ratio of 0.5, 1, and 2 wt% are denoted as 0.5-Pt/MC, 1-Pt/MC, and 2-Pt/MC, respectively.

To obtain the Pt/MC paste, 150 mg of Pt/MC powder were mixed with 7 mL of n-butanol and 0.15 mL of tetrabutyl titanate. The Pt/MC counter electrodes were fabricated by coating Pt/MC paste on FTO conducting glass. Then the electrode was sintered at 400°C for 15 minutes. The carbon loading is about 150 μg/cm^2 for all Pt/MC electrodes. Therefore, the amounts of Pt for 0.5-Pt/MC electrode, 1-Pt/MC electrode, and 2-Pt/MC electrode were about 0.75 μg/cm^2, 1.5 μg/cm^2, and 3 μg/cm^2, respectively.

A colloidal TiO_2 suspension was prepared by hydrolysis of titanium isopropoxide precursor in aqueous solution of pH 2 under vigorous stirring at 80°C. The suspension was then autoclaved at 250°C for 12 hours and condensed in a rotary evaporation. The TiO_2 electrode with the thickness of 10 μm was fabricated by depositing TiO_2 colloidal paste on FTO conducting glass substrate using doctor-blading method and then sintered at 450°C for 30 minutes in air. After cooling to 80°C, the TiO_2 electrode was immersed into the solution of cis-di(thiocyanato)-N,N′-bis(4, 4′-dicarrboxylate-2, 2′-bipyridyl) ruthenium(II) in ethanol for 12 hours at room temperature. The

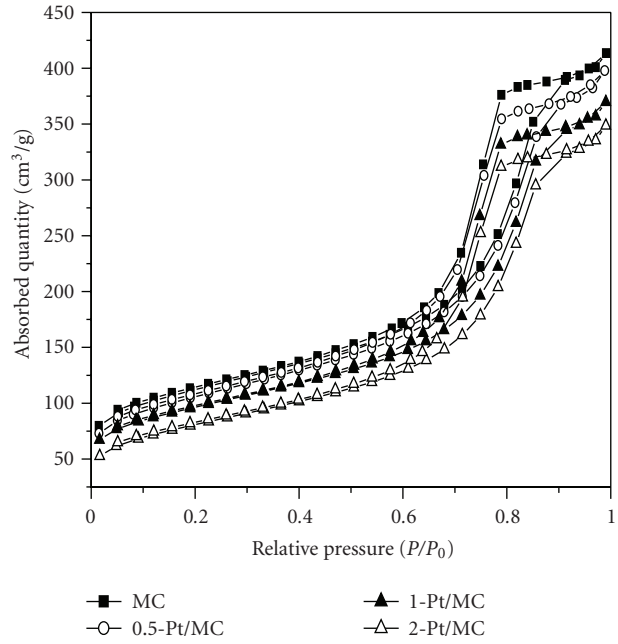

Figure 1: The N_2 adsorption-desorption isotherm of the as-prepared MC, 0.5-Pt/MC, 1-Pt/MC, and 2-Pt/MC samples.

DSCs were assembled by sandwiching the dye-sensitized TiO_2 electrode and counter electrode with a 25 μm thick spacer. The electrolyte was introduced into the cell by capillary effect through the thin cap between the two electrodes.

Nitrogen adsorption measurements were carried out at 77 K with a Micromeritics ASAP 2010 instrument. The surface area and the pore volume were determined using the Brunauer-Emmett-Teller (BET) equation and the single point method, respectively. The pore size distribution was calculated by Barrett-Joyner-Halenda (BJH) method. TEM images of samples were obtained with a Philips CM30 TEM. X-ray diffraction patterns were obtained using a Rigaku D/max B diffractometer with Cu Kα radiation. X-ray photoelectron spectroscopy data were obtained with an ESCALab220i-XL electron spectrometer using 300 W AlKα radiation.

The interfacial charge-transfer performance of Pt/MC counter electrode was determined by electrochemical impedance spectroscopy (EIS). EIS measurements were performed with a CHI660C electrochemical station in a symmetric thin-layer cell consisting of two identical Pt/MC counter electrode. The thin-layer cell was filled with electrolyte containing 0.5 M KI/0.05 M I_2 in the mixture of ethylene carbonate (EC) and propylene carbonate (PC) (EC : PC = 2 : 8 by volume). The current-voltage characteristics of DSCs were measured using a Keithley 2611 system sourcemeter under irradiation of 100 mW/cm^2 (AM1.5). A 1000 W Newport solar simulator fitted with an AM 1.5 global filter was employed as the light source. The active area of the cell was 0.25 cm^2.

Table 1: Surface area, average pore size, and pore volume for MC and Pt/MC samples and the specific surface area of Pt particles for Pt/MC samples.

Sample	Surface area (m^2/g)	Average pore size (nm)	Pore volume (cm^3/g)	S_{TEM} (m^2/g)
MC	380	8.6	0.64	
0.5-Pt/MC	370	8.2	0.61	93.02
1-Pt/MC	355	7.8	0.59	82.27
2-Pt/MC	323	7.5	0.57	68.22

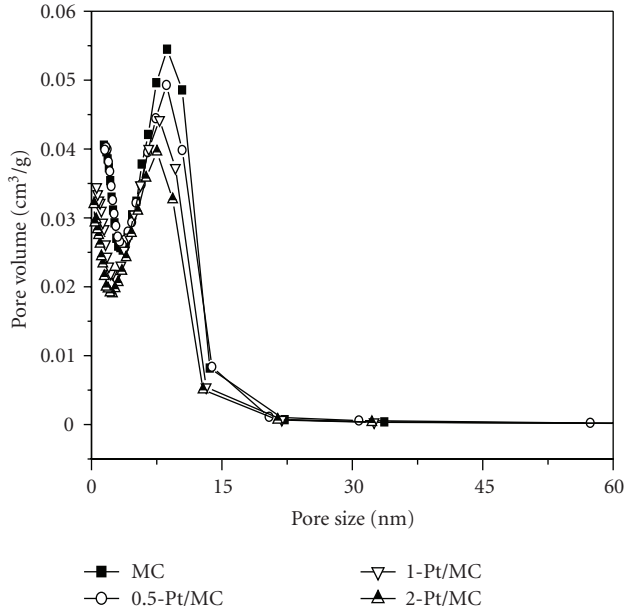

Figure 2: The pore size distribution curve of the as-prepared MC, 0.5-Pt/MC, 1-Pt/MC, and 2-Pt/MC samples.

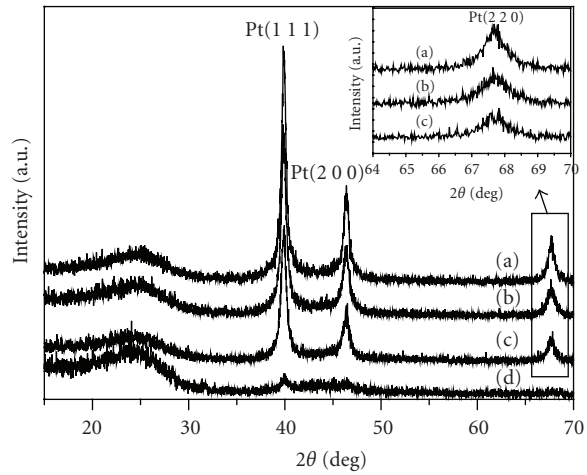

Figure 3: XRD patterns of MC (d), 0.5-Pt/MC (c), 1-Pt/MC (b), and 2-Pt/MC (a) samples. The inset is the detail scan of Pt(2 2 0) peaks for Pt/MC samples.

3. Results and Discussion

The Nitrogen adsorption studies were carried out on the as-prepared MC and Pt/MC samples. Nitrogen adsorption-desorption isotherms of MC and Pt/MC samples are depicted in Figure 1. As shown in Figure 1, the carbon sample displays type IV isotherm with a pronounced hysteresis loop at medium relative pressure, indicating the mesoporous structure of carbon sample. As compared with isotherm of MC samples, the isotherms of 0.5-Pt/MC, 1-Pt/MC, and 2-Pt/MC show similar pattern with reduced volume absorbed. This result indicates that the mesoporous structures are preserved in Pt/MC samples. Figure 2 shows the pore size distribution curve of as-prepared MC and Pt/MC samples. The pore size distribution of MC and Pt/MC samples displays the graph with one narrow peak. With the increase of the Pt loading, the peak of pore size distribution curves shifts to smaller pore size and the peak intensities decrease, which is probably related to the monolayer Pt loading on the MC surface and subsequent pore filling which in turn reflects the Pt loading inside the pore of MC samples. The structural parameters for both MC and Pt/MC samples are presented in Table 1. The surface area, the average pore size, and the pore volume of MC support are 380 m^2/g, 8.6 nm, and 0.63 m^3/g, respectively. The large surface area, together with the large pore size (>6 nm), makes as-prepared MC well suited to the support for Pt catalyst. As expected, the surface area, the average pore size, and the pore volume decrease slightly as the Pt contents in the Pt/MC samples are increased.

Figure 3 shows the XRD patterns of MC and Pt/MC samples. One broad diffraction peak around $2\theta = 23°$ belongs to the MC support. All XRD patterns of Pt/MC samples exhibit the characteristic diffraction peaks of Pt(1 1 1) at $2\theta = 39.8°$, Pt(2 0 0) at $2\theta = 45.88°$, and P(2 2 0) at $2\theta = 67.88$, indicating that Pt is present in the face centered cubic (FCC) phase. The inset in Figure 3 shows the detail scan of Pt(2 0 0) peaks. It gets narrower with the increase of the Pt loading, indicating that the average size of Pt particles becomes larger. The TEM images of Pt/MC samples are shown in Figure 4. From Figure 4, it is observed that the Pt particles disperse uniformly on the MC support. The average size of Pt particles for 0.5-Pt/MC, 1-Pt/MC, and 2-Pt/MC samples calculated from the measurement of randomly taken 100–200 particles are about 3 nm, 3.4 nm, and 4.1 nm, respectively. The pore size of MC support is more than twice Pt particles. Therefore, the Pt particles in the pore of MC support are unable to contact each other and the pore blockage will not occur in this case, resulting in the excellent accessibility of Pt particles. The specific area of Pt particles (S_{TEM}) can be calculated

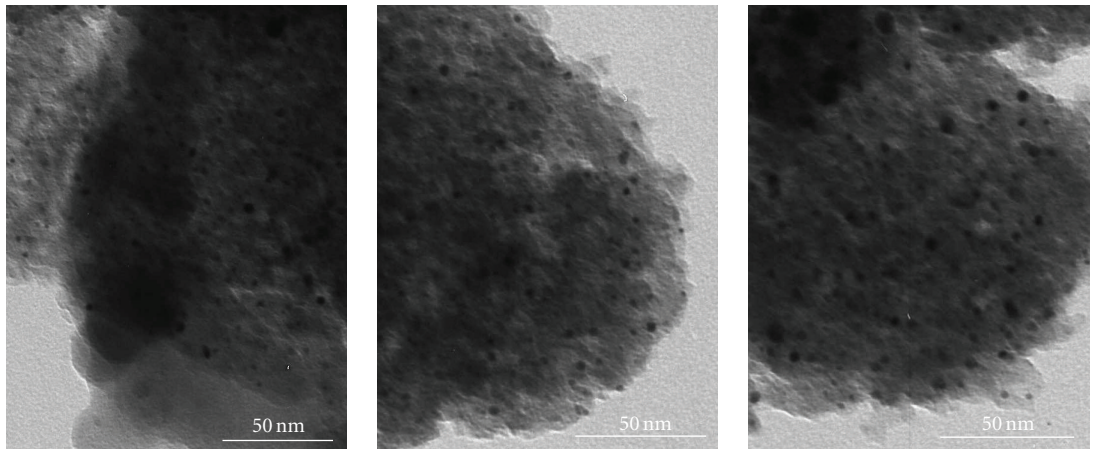

Figure 4: TEM images of 0.5-Pt/MC (a), 1-Pt/MC (b), and 2-Pt/MC (c) samples

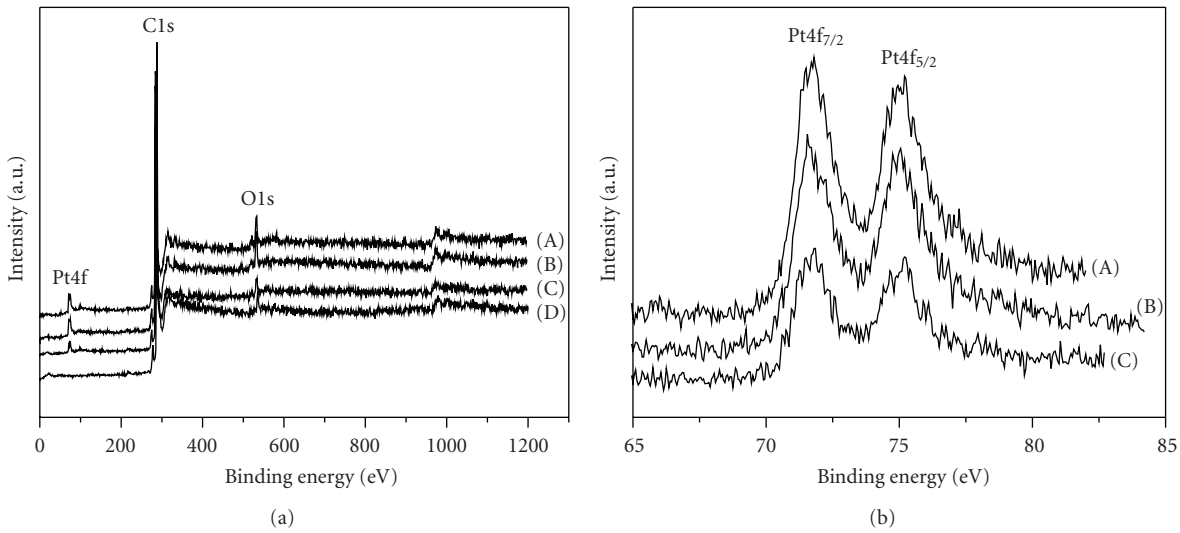

Figure 5: The XPS survey spectra (a) and the Pt4f spectra (b) for as-prepared MC (D), 0.5-Pt/MC (C), 1-Pt/MC (B), and 2-Pt/MC (A) samples.

with the particles size from TEM analysis according to the following equation [27]:

$$S_{\mathrm{TEM}} = \frac{6 \times 10^3}{\phi \rho_{\mathrm{Pt}}}, \quad (1)$$

where ϕ (nm) is the average particle size from TEM and ρ_{Pt} is the Pt density (21.45 g/cm^3). The S_{TEM} for the Pt/MC samples calculated using the above equation was described in Table 1. The S_{TEM} for 0.5-Pt/MC, 1-Pt/MC, and 2-Pt/MC samples is 93.02, 82.27, and 68.22 m^2/g, respectively. The high S_{TEM} along with the excellent accessibility of Pt particles means the high utilization efficiency of Pt catalyst.

The electronic state of Pt for Pt/MC samples is determined by XPS. Figure 5 shows the XPS survey spectra and the Pt4f XPS spectra of MC and Pt/MC samples. As shown in Figure 5(a), the Pt, C, and O signals are observed in the XPS survey spectra of Pt/MC samples, while only C and O peaks are observed in the XPS survey spectra of MC. The intensity of Pt peak is enhanced with the increase of the Pt loading. Figure 5(b) displays the Pt4f core level spectra of Pt/MC samples. Considering all Pt/MC samples, the intensive doublet (at ca. 71.6 and 74.9 eV) indicates the metallic Pt. The slight shift of the Pt4f$_{7/2}$ and Pt4f$_{5/2}$ peaks to the higher binding energies might be a signal of stronger MC support/Pt interaction.

The interfacial charge-transfer performance of Pt/MC counter electrodes was studied by applying EIS. The electrochemical impedance spectra of the symmetric thin-layer cell consisted of two identical Pt/MC electrodes are shown in Figure 6. The equivalent circuit for this type of cell is illustrated in Figure 7. The ohmic series resistance (R_s) can be determined according to the high frequency of the impedance where the phase is zero. The impedance in the middle frequency range of 100 Hz–100 KHz is dominated

Table 2: The open-circuit voltage, the short-circuit current density, the fill factor, and the overall conversion efficiency of DSCs using the Pt/MC counter electrode with different Pt loading.

Pt loading (wt%)	V_{oc} (V)	J_{sc} (mA/cm^2)	FF	η (%)
0	0.605	12.8	0.56	4.33
0.5	0.61	14.65	0.6	5.36
1	0.635	17.11	0.61	6.62
2	0.63	17.21	0.61	6.61

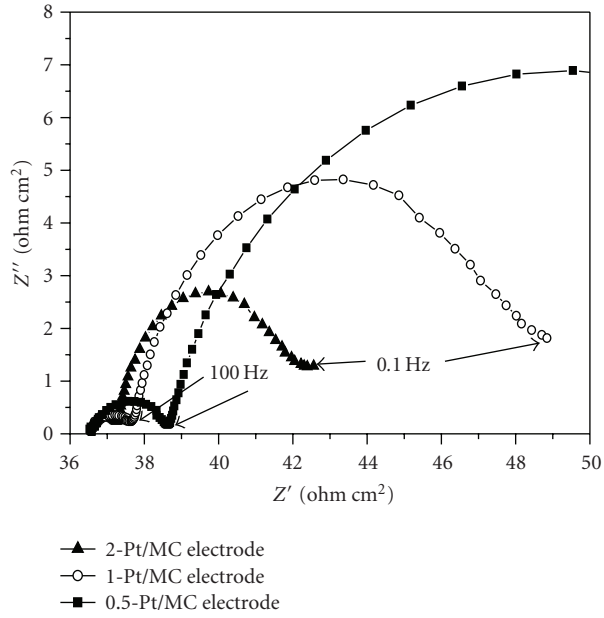

Figure 6: Electrochemical impedance spectra of the symmetric thin-layer cell consisting of two identical Pt/MC electrodes taken at zero bias, ac amplitude 10 mV, the electrolyte containing 0.5 M KI/0.05 M I_2 in the mixture of EC and PC (EC:PC = 2:8 by volume).

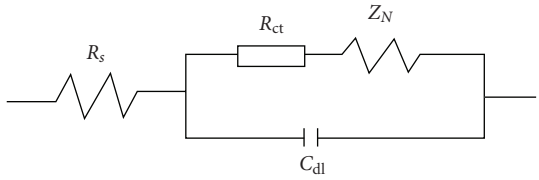

Figure 7: Equivalent circuit for the electrochemical impedance spectra in Figure 6 (R_s: Ohmic series resistance, R_{ct}: The charge-transfer resistance, C_{dl}: Capacitance of electric double layer, and Z_N: Nernst diffusion impedance).

by RC network of the Pt/MC electrode/electrolyte interface, consisting of charge-transfer resistance (R_{ct}) and the capacity of the electrical double layer. The impedance in the low-frequency range of 0.1–100 Hz can be attributed to the Nernst diffusion impedance. The R_{ct}, which characterize the electrocatalytic activity of Pt/MC electrodes for reduction of triiodide, can be directly obtained from the diameter of the semicircle in the frequency range of 100 Hz–100 KHz in the

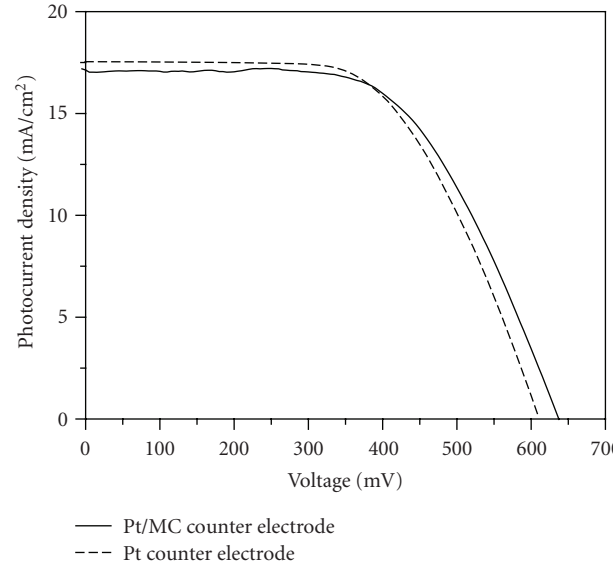

Figure 8: Photocurrent-voltage characteristics of DSCs with different counter electrode measured in the electrolyte as in Figure 6.

spectra. From the spectra shown in Figure 6, it is observed that the size of the semicircle decreases with the increase of Pt loading. The R_{ct} of 2.5 Ωcm^2 for 0.5-Pt/MC electrode, the R_{ct} of 1.2 Ωcm^2 for 1-Pt/MC electrode, and the R_{ct} of 0.8 Ωcm^2 for 2-Pt/MC electrode are determined.

Table 2 summarizes the photovoltaic parameters of the DSCs using Pt/MC counter electrode with different Pt loading. It can be seen that the photovoltaic performance of DSCs with Pt/MC counter electrode is improved with the increase of Pt content in MC. When an MC electrode without Pt is used as counter electrode, the open-circuit voltage (V_{oc}), the short-circuit current density (J_{sc}), the fill factor (FF), and the overall conversion efficiency (η) of DSCs are only 0.605 V, 12.8 mA/cm^2, 0.56, and 4.33%, respectively. While 1-Pt/MC electrode is used as a counter electrode, the V_{oc}, the J_{sc}, and the FF of DSCs increase to 0.635 V, 17.11 mA/cm^2 and 0.61, respectively, and the overall conversion efficiency is up to 6.62%. The average conversion efficiency for a batch of eight separate devices was 6.62 ± 0.09%. Furthermore, no apparent difference in V_{oc}, J_{sc} and η is observed between DSCs with 1-Pt/MC counter electrode and DSCs with 2-Pt/MC counter electrode. Therefore, the 1 wt% Pt loading on MC is sufficient for catalyzing the reduction of triiodide at the interface between counter electrode and electrolyte.

Table 3: The photovoltaic parameters of DSCs with 1-Pt/MC counter electrode and the conventional Pt counter electrode.

Counter electrode	V_{oc} (V)	J_{sc} (mA/cm^2)	FF	η (%)
1-Pt/MC	0.635	17.11	0.61	6.62
Pt	0.611	17.52	0.60	6.42

Figure 8 shows the photocurrent-voltage curve of DSCs with 1-Pt/MC counter electrode and the conventional Pt counter electrode. Pt counter electrode is prepared by the thermal decomposition of H_2PtCl_6 on FTO glass, the Pt loading is about 6 μg/cm^2 [28]. The photovoltaic parameters are summarized in Table 3. The overall conversion efficiency of DSCs with 1-Pt/MC counter electrode is higher than that of the cell with Pt counter electrode. The Pt loading in 1-Pt/MC counter electrode is only about 1.5 μg/cm^2, which is much lower than that of 6 μg/cm^2 commonly used for Pt counter electrode in DSCs. Therefore, the highly dispersed Pt/MC with a low Pt loading provides the possibility of cost reduction for high-efficiency DSCs.

The stability of DSCs with 1-Pt/MC counter electrode is studied by monitoring the photocurrent-voltage characteristics with time under continuous illumination. No obvious change for the photoelectric parameter of DSCs with 1-Pt/MC counter electrode was observed during test within three weeks. This result indicates that the low-Pt-loading Pt/MC electrode is feasible for DSCs with high-conversion efficiency.

4. Conclusion

Pt/MC samples with a low Pt loading were prepared by reducing H_2PtCl_6 with $NaBH_4$ in synthesized MC support. Pt nanoparticles highly dispersed in MC support present as metallic platinum. With the increase of the Pt loading, the size of Pt particles on the surface of MC increased slightly. Pt/MC counter electrodes for DSCs were fabricated by coating Pt/MC paste on FTO conducting glass. The Pt loading in as-prepared Pt/MC electrode is only about 0.75–3 μg/cm^2, which is much lower than 6 μg/cm^{-2} generally used for the Pt electrode in DSCs. Electrochemical measurements display a low R_{ct} of 1.2 Ωcm^2 for 1-Pt/MC counter electrode (with Pt loading of 1.5 μg/cm^2). An overall conversion efficiency of 6.62% is obtained for DSCs with 1-Pt/MC counter electrode, which is higher than that of DSCs with conventional Pt counter electrode. We believe that this novel counter electrode could be very useful for reducing the manufacturing cost of DSCs and improving the photovoltaic performance of DSCs.

Acknowledgments

This work is supported by National Natural Science Foundation of China (no. 20773082) and Shandong Department of Science and Technology (no. 2006BS09003).

References

[1] B. O'Regan and M. Grätzel, "A low-cost, high-efficiency solar cell based on dye-sensitized colloidal TiO_2 films," *Nature*, vol. 353, no. 6346, pp. 737–740, 1991.

[2] M. Grätzel, "Perspectives for dye-sensitized nanocrystalline solar cells," *Progress in Photovoltaics: Research and Applications*, vol. 8, no. 1, pp. 171–185, 2000.

[3] X. Zhang, H. Yang, H.-M. Xiong, F.-Y. Li, and Y.-Y. Xia, "A quasi-solid-state dye-sensitized solar cell based on the stable polymer-grafted nanoparticle composite electrolyte," *Journal of Power Sources*, vol. 160, no. 2, pp. 1451–1455, 2006.

[4] K. Kalyanasundaram and M. Grätzel, "Applications of functionalized transition metal complexes in photonic and optoelectronic devices," *Coordination Chemistry Reviews*, vol. 177, no. 1, pp. 347–414, 1998.

[5] N. Papageorgiou, P. Liska, A. Kay, and M. Grätzel, "Mediator transport in multilayer nanocrystalline photoelectrochemical cell configurations," *Journal of the Electrochemical Society*, vol. 146, no. 3, pp. 898–907, 1999.

[6] N. Papageorgiou, W. F. Maier, and M. Grätzel, "An iodine/triiodide reduction electrocatalyst for aqueous and organic media," *Journal of the Electrochemical Society*, vol. 144, no. 3, pp. 876–884, 1997.

[7] A. Hauch and A. Georg, "Diffusion in the electrolyte and charge-transfer reaction at the platinum electrode in dye-sensitized solar cells," *Electrochimica Acta*, vol. 46, no. 22, pp. 3457–3466, 2001.

[8] A. Zaban, J. Zhang, Y. Diamant, O. Melemed, and J. Bisquert, "Internal reference electrode in dye sensitized solar cells for three-electrode electrochemical characterizations," *Journal of Physical Chemistry B*, vol. 107, no. 25, pp. 6022–6025, 2003.

[9] E. Ramasamy, W. J. Lee, D. Y. Lee, and J. S. Song, "Spray coated multi-wall carbon nanotube counter electrode for tri-iodide (I3-) reduction in dye-sensitized solar cells," *Electrochemistry Communications*, vol. 10, no. 7, pp. 1087–1089, 2008.

[10] K. Suzuki, M. Yamaguchi, M. Kumagai, and S. Yanagida, "Application of carbon nanotubes to counter electrodes of dye-sensitized solar cells," *Chemistry Letters*, vol. 32, no. 1, pp. 28–29, 2003.

[11] C.-S. Chou, R.-Y. Yang, M.-H. Weng, and C.-I. Huang, "The applicability of SWCNT on the counter electrode for the dye-sensitized solar cell," *Advanced Powder Technology*, vol. 20, no. 4, pp. 310–317, 2009.

[12] H. J. Choi, J. E. Shin, G.-W. Lee, N.-G. Park, K. Kim, and S. C. Hong, "Effect of surface modification of multi-walled carbon nanotubes on the fabrication and performance of carbon nanotube based counter electrodes for dye-sensitized solar cells," *Current Applied Physics*, vol. 10, no. 2, pp. S165–S167, 2010.

[13] J. G. Nam, Y. J. Park, B. S. Kim, and J. S. Lee, "Enhancement of the efficiency of dye-sensitized solar cell by utilizing carbon nanotube counter electrode," *Scripta Materialia*, vol. 62, no. 3, pp. 148–150, 2010.

[14] K. Imoto, K. Takahashi, T. Yamaguchi, T. Komura, J.-I. Nakamura, and K. Murata, "High-performance carbon counter electrode for dye-sensitized solar cells," *Solar Energy Materials and Solar Cells*, vol. 79, no. 4, pp. 459–469, 2003.

[15] T. N. Murakami, S. Ito, Q. Wang et al., "Highly efficient dye-sensitized solar cells based on carbon black counter electrodes," *Journal of the Electrochemical Society*, vol. 153, no. 12, pp. A2255–A2261, 2006.

[16] Z. Huang, X. Liu, K. Li et al., "Application of carbon materials as counter electrodes of dye-sensitized solar cells," *Electrochemistry Communications*, vol. 9, no. 4, pp. 596–598, 2007.

[17] J. Wu, Q. Li, L. Fan et al., "High-performance polypyrrole nanoparticles counter electrode for dye-sensitized solar cells," *Journal of Power Sources*, vol. 181, no. 1, pp. 172–176, 2008.

[18] Y. Saito, W. Kubo, T. Kitamura, Y. Wada, and S. Yanagida, "I^-/I_3^- redox reaction behavior on poly (3,4-ethylenedioxythiophene) counter electrode in dye-sensitized solar cells," *Journal of Photochemistry and Photobiology A*, vol. 164, no. 1–3, pp. 153–157, 2004.

[19] S.-S. Kim, K.-W. Park, J.-H. Yum, and Y.-E. Sung, "Pt-NiO nanophase electrodes for dye-sensitized solar cells," *Solar Energy Materials and Solar Cells*, vol. 90, no. 3, pp. 283–290, 2006.

[20] G. Khelashvili, S. Behrens, C. Weidenthaler et al., "Catalytic platinum layers for dye solar cells: a comparative study," *Thin Solid Films*, vol. 511-512, pp. 342–348, 2006.

[21] B. M. Babić, L. M. Vračar, V. Radmilović, and N. V. Krstajić, "Carbon cryogel as support of platinum nano-sized electrocatalyst for the hydrogen oxidation reaction," *Electrochimica Acta*, vol. 51, no. 18, pp. 3820–3826, 2006.

[22] D. He, L. Yang, S. Kuang, and Q. Cai, "Fabrication and catalytic properties of Pt and Ru decorated TiO_2-CNTs catalyst for methanol electrooxidation," *Electrochemistry Communications*, vol. 9, no. 10, pp. 2467–2472, 2007.

[23] A. L. Dicks, "The role of carbon in fuel cells," *Journal of Power Sources*, vol. 156, no. 2, pp. 128–141, 2006.

[24] S.-K. Kang, S.-W. Lee, and H.-C. Ryu, "Palladium- and copper-catalyzed cross-coupling and carbonylative cross-coupling of organotellurium compounds with organostannanes," *Chemical Communications*, no. 20, pp. 2117–2118, 1999.

[25] R. Ryoo, S. H. Joo, and S. Jun, "Synthesis of highly ordered carbon molecular sieves via template-mediated structural transformation," *Journal of Physical Chemistry B*, vol. 103, no. 37, pp. 7745–7746, 1999.

[26] G. Wang, W. Xing, and S. Zhuo, "Application of mesoporous carbon to counter electrode for dye-sensitized solar cells," *Journal of Power Sources*, vol. 194, no. 1, pp. 568–573, 2009.

[27] B. Le Gratiet, H. Remita, G. Picq, and M. O. Delcourt, "CO-stabilized supported Pt catalysts for fuel cells: radiolytic synthesis," *Journal of Catalysis*, vol. 164, no. 1, pp. 36–43, 1996.

[28] N. Papageorgiou, W. F. Maier, and M. Grätzel, "An iodine/triiodide reduction electrocatalyst for aqueous and organic media," *Journal of the Electrochemical Society*, vol. 144, no. 3, pp. 876–884, 1997.